Reducing PDK4 level constitutes a pivotal mechanism for glucocorticoids to impede osteoblastic differentiation through the enhancement of ferroptosis in mesenchymal stem cells

Yue Jiang[1,2†], Ai-Hua Ye[1,2†], Wen-Ge He[2,3,4†], Lu Liu[1,2], Xiang Gao[2,5], Hang Liu[2,5], Wen-Ting Liu[1,2], Fang-Lin Ye[1,2], Dong-Mei He[1,2], Jun-Yi Liao[3], Jing Wang[6*] and Bai-Cheng He[1,2*]

Abstract

Background This study mainly explores the possible role and mechanism of pyruvate dehydrogenase kinase 4 (PDK4) in the onset and development of Glucocorticoid-induced osteoporosis (GIOP), and seeks potential targets for the treatment of GIOP.

Methods Mesenchymal stem cells (MSCs) were treated with osteogenic induction medium. An in vitro osteogenic damage model was established by exposing MSCs to a high concentration (10^{-6} M) of dexamethasone (DEX). Osteogenic markers were measured with real-time quantitative polymerase chain reaction, western blot, alkaline phosphatase staining, and Alizarin Red S staining. Ferroptosis markers were assessed through reactive oxygen species (ROS) fluorescent probe, transmission electron microscopy, and measurement of malondialdehyde (MDA). The potential mechanism was investigated using RT-qPCR, western blot, lysosomal probes, molecular docking, and other analytical approaches. The role of PDK4 was validated by using a GIOP rat model, micro-computed tomography and Masson's trichrome staining.

Results High concentrations (10^{-6} M) of DEX inhibited osteogenic differentiation in C3H10T1/2 cells, and PDK4 exhibited the opposite effect. PDK4 partially reversed the osteogenic inhibitory effect of DEX both in vivo and in vitro. DEX caused mitochondrial shrinkage and disappearance of cristae in C3H10T1/2 cells, as well as an increase in total iron, ROS, MDA contents, and the level of ferroptosis key factors. These changes were partially weakened by PDK4. The ferroptosis inhibitor ferrostatin-1 partially blocked the inhibitory effect of DEX, while ferroptosis inducer RSL3 inhibited

†Yue Jiang, Ai-Hua Ye and Wen-Ge He have equally contributed.

*Correspondence:
Jing Wang
wjsy86@hospital.cqmu.edu.cn
Bai-Cheng He
bche@cqmu.edu.cn

Full list of author information is available at the end of the article

Jiang *et al. Stem Cell Research & Therapy*   (2025) 16:91

Page 2 of 20

osteogenic differentiation and weakened the reversal effect of PDK4. DEX reduced the protein level of PDK4, which was partially weakened by Bafilomycin A1. The molecular docking results showed that DEX can directly bind with PDK4.

Conclusion PDK4 can enhance the osteogenic differentiation ability of MSCs and bone mass of GIOP rats. DEX may promote the degradation of PDK4 via lysosome pathway, through which to weaken the osteogenic ability of MSCs by increasing ferroptosis. PDK4 may become a potential target for improving GIOP.

Keywords Glucocorticoid-induced osteoporosis (GIOP), Dexamethasone, Osteogenic differentiation, Pyruvate dehydrogenase kinase 4, Ferroptosis

Background

Glucocorticoid-induced osteoporosis (GIOP) is a common adverse reaction after long-term and high-dose use of glucocorticoids (GCs) such as dexamethasone, and is also the most common secondary osteoporosis [1]. The main pathological features of GIOP are sustained reduction in bone formation and increased bone resorption, culminating in loss of bone mass [2]. The incidence of fractures in patients is related to the duration and dosage of GCs usage [3]. High doses of GCs can exert inhibitory effects on osteoblast proliferation and disrupt osteogenic differentiation of mesenchymal stem cells (MSCs) primarily by suppressing BMP/Smads and phosphatidylinositol 3 kinase/protein kinase B (PI3K/Akt) signaling pathways [4, 5]. DEX mainly inhibits osteoblast proliferation and prevents Wnt/β-catenin signaling pathway to reduce osteogenic differentiation of MSCs [6–9]. The GCs-induced ferroptosis in osteoblasts and autophagy in osteoblasts and osteoclasts are involved in occurrence and development of osteoporosis [10–14]. Therefore, searching for the crucial mechanisms and potential therapeutic targets of GIOP remains of great clinical significance.

Aerobic glycolysis plays an important role in the osteogenic differentiation of MSCs [15, 16]. Pyruvate dehydrogenase kinase 4 (PDK4) is a key enzyme that regulates the activity of the pyruvate dehydrogenase complex (PDC) by phosphorylating its subunits, and thereby reduces the conversion of pyruvate to acetyl CoA and promoting glycolysis [17–19]. It was reported that PDK4 plays an important role in promoting calcification in vascular smooth muscle cells, which may be related to interact with phosphorylated Smad1/5/8 [20], mitochondrial function, and changes in autophagy [21, 22]. Given the similarity between vascular calcification and bone formation processes, we previous found that PDK4 can promote the osteogenic induction potential of bone morphogenetic protein 9 [23]. However, the impact of PDK4 on DEX-induced osteogenic inhibition and whether it can become a potential target for treating GIOP is still unclear.

Ferroptosis, another form of cell death marked by iron overload and the accumulation of reactive oxygen species (ROS), involves diverse biological pathways encompassing iron and lipid metabolism, oxidative stress, and the synthesis of glutathione and coenzyme Q10 [24, 25]. Ferroptosis may be closely related to the occurrence and development of orthopedic diseases, such as osteoporosis, osteosarcoma and osteoarthritis [26]. The level of critical proteins associated with ferroptosis, such as SLC7A11 and GPX4, in femur protein of osteoporosis model rats fed with high sugar or high-fat diet was abnormal, and ferroptosis inhibitors can partially reverse the bone loss caused by high-fat diet [27]. Jiang et al. revealed that iron overload can inhibit osteogenic differentiation by inducing ferroptosis in MC3T3-E1 cells [28]. Luo et al. also demonstrated that induction of iron overload in BMSCs via ferric ammonium citrate can inhibit osteogenic differentiation by interfering with Wnt/β-catenin signaling [29]. In addition, GCs can induce ferroptosis in MSCs, and melatonin can alleviate GIOP by inhibiting ferroptosis in BMSCs through PI3K/AKT/mTOR signaling [30–32]. PDK4 can inhibit ferroptosis which making it become an important potential anti-cancer target [33]. However, the link between PDK4 and ferroptosis in MSCs necessitates further investigation.

In this study, we performed in vitro and in vivo experiments to explore the connection between glucocorticoid-induced bone damage and PDK4. This research endeavor holds the potential to unravel novel therapeutic targets for the management of GIOP.

Materials and methods

Cell culture and chemicals

HEK293, C3H10T1/2, MEFs, C2C12, MC3T3-E1, and MC3T3-L1 cells were procured from ATCC (Manassas, VA, USA). These cells were cultured in Dulbecco's modified Eagle's medium supplemented with glucose (4.5 g/L) and 10% fetal bovine serum, alongside penicillin (100 U/mL) and streptomycin (100 μg/mL), maintained at 37 °C in 5% CO_2. Materials, including DMEM (SMK200.01), FBS (SMK100.01), trypsin (SMK0104), and PBS (SMK0106), were acquired from Saimike (Chongqing, China). Primary antibodies targeting β-Actin (AC038), PDK4 (A13337), ACSL4 (A20414), and FTH1 (A19644) were purchased from ABclonal (Wuhan,

China). Additionally, OPN (sc-21742) and BMP9 (sc-514211) were procured from Santa Cruz Biotechnology's Chinese branch, while RUNX2 (TA5186), GPX4 (T56959), and xCT/SLC7A11 (T57046) were obtained from Abmart (Shanghai, China). Substances such as dexamethasone (ST1254) were sourced from Beyotime (Shanghai, China), while RSL3 (HY-100218 A) and Ferrostatin-1 (HY-100579) were acquired from MedChemExpress (Shanghai, China). Erastin (E872563) was procured from Macklin (Shanghai, China).

Recombinant adenovirus construction
The recombinant adenoviruses employed in this study were generated based on the AdEasy system. Coding sequences for PDK4, BMP9, GFP, RFP were amplified through polymerase chain reaction (PCR). The products and PDK4 small interfering RNA subsequently cloned into the shuttle vector of the adenovirus. Subsequently, we recombined the shuttle vector with BJ5183/AdEasy-1 cells, followed by transduction for packaging in HEK293 cells. These recombinant adenoviruses were designated as AdBMP9, AdPDK4, AdGFP, AdRFP, and AdsiPDK4. Notably, green fluorescent protein (GFP) or red fluorescent protein (RFP) were utilized as viral tracking labels. AdGFP or AdRFP were used as vehicle controls.

Table 1 Primer sequence for this study

Gene	GeneBank entry	Primer	Sequence (5′→3′)
β-actin	NM_007393.5	F	CCACCATGTACCCAGGCATT
		R	CGGACTCATCGTACTCCTGC
Runx2	NM_001145920.1	F	GCCGGGAATGATGAGAACTA
		R	GGACCGTCCACTGTCACTTT
OPN	NM_001204233.1	F	TGCACCCAGATCCTATAGCC
		R	CTCCATCGTCATCATCATCG
PDK4	NM_013743.2	F	CTGCCTGACCGCTTAGTGAA
		R	TGCCTTGAGCCATTGTAGGG
PDK3	NM_145630.3	F	CTGCTCTAGTGAGGATGCGG
		R	TTAGCCAGTCGCACAGGAAG
PDK2	NM_001361915.1	F	GGTGAAACTGGGTCTCCCTG
		R	GAGAAGTGTCTCTGGGCCAC
PDK1	NM_001360002.1	F	AGGCTACATGTACGGACCCT
		R	GCCACCTCTCCTTTCAAGCT
FTH1	NM_010239.2	F	GCGGTTTCCTGCTTCAACAG
		R	GTCCTGGTGGTAGTTCTGGC
SLC7A11	NM_011990.2	F	GGAAGTCACGACCGAACAGT
		R	ATTGCCCTGCAGGTAACCTC
GPX4	NM_001367995.1	F	ATGAAAGTCCAGCCCAAGGG
		R	GTGTAGGGGCACACACTTGT
ACSL4	NM_207625.2	F	GGAAAGCAAACTGAAGGCGG
		R	AATGGCCATGTCTGAAGGGG

(F: forward, R: reverse)

Preparation of osteogenic induction medium
The osteogenic induction medium (OIM) is formulated by supplementing DMEM with β-glycerophosphate, dexamethasone, and L-ascorbic acid. The specific preparation involves dissolving these three components in DMEM, followed by filtrating using a sterile 0.2 µm filter. The final concentration of each component are adjusted to 10 mM for β-glycerophosphate, 100 nM for dexamethasone, and 250 µM for L-ascorbic acid [34].

RNA extraction, reverse transcription (RT), and real time polymerase chain reaction (PCR)
Total RNA was extracted using TRIzol reagent (15596026; Invitrogen, USA), and the quality and concentration were assessed using the NanoDrop One machine (Thermo Fisher Scientific, USA). Subsequently, the extracted RNA underwent reverse transcription using RT Kits (RR037A; Takara), and the products were diluted 5 to 10 times to act as templates for the PCR assay. Real-time quantitative PCR was performed using the 2x SYBR Green qPCR Master Mix Kit (B2120, Selleck, USA) and the Bio-Rad CFX Connect System (Bio-Rad, Chicago, USA), following this thermal cycling profile: pre-denaturation at 95℃ for 3 min, denaturation at 95℃ for 10 s, annealing at 58℃ for 30 s and extension at 72℃ for 10 s, repeated for 40 cycles. The relative gene expression levels were calculated using the $2^{-\Delta\Delta Ct}$ method and normalized to the levels of β-actin. The primers utilized in this study were shown in Table 1.

Protein collection and Western blot analysis
Cells were initially seeded in 6-well plates or cell culture dishes, followed by treatment with various factors as following the experimental design. At designated time points, cells in the wells were washed twice with 4 °C pre-chilled phosphate buffered saline (PBS), and followed by lysising for 5 to 10 min on ice using RIPA lysis buffer (ST506, Beyotime, Shanghai, China) containing 1% PMSF (P0013B, Beyotime, Shanghai, China). Lysates were then scraped and collected into 1.5 mL tubes. Protein loading buffer (P0015L, Beyotime, Shanghai, China) was added, and the samples were boiled in a water bath for 15 min. The samples were separated using 10% or 12.5% SDS-PAGE and subsequently transferred to PVDF membranes (Bio-Rad, USA). Blocking was performed at room temperature for 30 min using a protein-free rapid blocking solution (Epizyme, Shanghai, China), followed by overnight incubation at 4 °C with primary antibodies. Membranes were washed four times with TBST (Tris-Buffered Saline, 0.1% Tween 20), then incubated for 1 h with the corresponding horseradish peroxidase-conjugated secondary antibodies (Beyotime, Shanghai, China). After four additional washes, detection was carried out using a chemiluminescent substrate kit (160072; Saimike,

Chongqing, China) and a gel imager (ChemiScope 6200, Qinxiang, China). Quantitative analysis was performed using ImageJ software.

Alkaline phosphatase (ALP) staining

C3H10T1/2 cells were seeded in 24-well plates and treated with various factors. After 5 or 7 days of differentiation induction with OIM, the cells were gently rinsed twice with PBS. Alkaline phosphatase (ALP) activity was then assessed using a BCIP/NBT Alkaline Phosphatase Color Development Kit (C3206, Beyotime, Shanghai, China). Following the staining process, cells were washed twice with PBS and air-dried. Plates were conducted using a scanner (Phentom, China) and Microtek Scan-Wizard 5 software. Additionally, images were captured under an optical microscope (IX53, Olympus, Tokyo, Japan).

Alizarin Red S (ARS) staining

Cells were cultured in 24-well plates and treated with various factors for osteogenic induction over 14 or 21 days. The culture medium was discarded, and cells were gently rinsed twice using PBS (pH 4.2). Cells were then fixed for 15 min with 4% paraformaldehyde followed by another rinse. Staining was performed for 20 min using a 0.2% Alizarin Red solution (G8550, Solarbio, Beijing, China). After washing with PBS, the samples were scanned using a Phentom scanner (China) and Microtek ScanWizard 5 software, and images were captured under an optical microscope (IX53, Olympus, Tokyo, Japan). Quantitative analysis was conducted using ImageJ software.

Construction of GIOP rat and delivery of AAV-PDK4

Animal experiments were approved by the Institutional Ethics Committee of Chongqing Medical University (IACUC-CQMU-2022-0021). Twenty male Sprague-Dawley (SD) rats, aged 8 weeks and each weighing approximately 200 g, were sourced from the Experimental Animal Center of Chongqing Medical University. The animals were individually placed in a rigorously controlled environment at the Chongqing Medical University's animal facility, adhering strictly to the protocols established by both the National Institutes of Health and the Institutional Animal Care and Use Committee. This facility featured with an automated temperature regulation system, maintaining a stable temperature range of 22 ± 2 °C and a relative humidity level of $50 \pm 10\%$. To mimic natural diurnal rhythms, the animals were subjected to a regulated 12-hour light-dark cycle. Each animal's cage was furnished with standard bedding materials, which were changed frequently, at least twice weekly, to uphold hygiene standards and deter the build-up of waste or potentially harmful microorganisms. To enhance the animals' psychological well-being

and alleviate boredom, they were provided with a range of environmental enrichment items, including nesting materials, chewable toys, and/or visual barriers. The animals had unrestricted access to a species-specific, balanced laboratory diet designed to meet their nutritional needs. An automated watering system ensured continuous access to fresh, filtered water. Trained personnel conducted daily health checks, monitoring the animals for signs of illness, injury, or distress. Any animal exhibiting abnormal behaviors or physiological alterations was promptly removed from the study and provided with necessary veterinary attention. Throughout the experimental period, the utmost priority was placed on ensuring the health and well-being of the animals.

Rats were randomly divided into 4 groups and five mice each group. After an one-week acclimatization period, they were further randomized into one control group and three GIOP experimental groups. The treatment for the experimental groups included intraperitoneal injection of dexamethasone sodium phosphate (5 mg/Kg) for 4 weeks to induce GIOP. The control group received intraperitoneal injections of an equivalent volume of normal saline. Approximately 8 weeks post-treatment initiation, the GIOP experimental groups were further subdivided into the PBS group, AAV-Vehicle group (virus empty vector group), and AAV-PDK4 group. Each rat in the AAV-PDK4 group received a tail vein injection of 200 μl solution containing 2×10^{12} v.g AAV-PDK4, while the AAV-Vehicle group received 200 μl of empty vector control (containing 2×10^{12} v.g AAV-GdGreen). The PBS group and the original control group received tail vein injections of an equivalent volume of PBS.

After 4 weeks, rats were anesthetized via intraperitoneal injection of 2% sodium pentobarbital (50 mg/kg, supplied by the Animal Experiment Center of Chongqing Medical University). Vital signs such as respiration and heart rate were closely observed to ensure adequate anesthesia depth and avoid any potential discomfort. Once the rats were successfully anesthetized, cardiac blood, femur, and tibiae were harvested for subsequent experiments. Upon completion of the experiments, rats were placed in a euthanasia chamber, where CO_2 gas was introduced at a flow rate corresponding to 60% volume displacement per minute. Once the rats lost consciousness, 100% CO_2 was administered for an additional 2 min until death was confirmed.

Lysosome co-localization assay

Cells were transfected with AdPDK4 tagged with GFP fluorescence. After 6 h, cells were treated with 1 μM DEX for 48 h. Following removal of the original culture medium, cells were incubated with 50 nM Lyso-Tracker Red (C1046, Beyotime, Shanghai, China) working solution to label lysosomes at 37 °C for 60 min. Subsequently,

the working solution was removed, and cells were washed three times with PBS for 5 min each. Hoechst stain solution (C1022, Beyotime, Shanghai, China) was then added to label cell nuclei, followed by incubation at room temperature in the dark for 10 min. Finally, cells were washed three times with PBS and fresh complete culture medium was added. PDK4 and lysosome co-localization were observed by confocal laser microscope (SP8, Leica, Wetzlar, Germany).

Histological evaluation and staining
The collected rat femurs were fixed in 4% paraformaldehyde for 3 days, decalcified in EDTA solution (pH 7.2) for 21 days, dehydrated in ethanol, and then embedded in paraffin. Samples were sectioned, and subjected to hematoxylin and eosin (H&E) staining and Masson's trichrome staining following deparaffinization and rehydration. Images were observed and captured using a microscope (Ci-L, Nikon, Tokyo, Japan).

Microcomputed tomography
The rat femurs were performed with computerized tomography scans (μCT) (SkyScan 1276, Bruker, Germany). Analysis was performed using the manufacturer's evaluation software. Reconstruction was accomplished by NRecon (version 1.7.4.2). Standard 3D microstructural analysis was used to evaluate parameters, including the trabecular BMD, bone volume fraction (BV/TV), trabecular thickness (Tb.Th), trabecular spacing (Tb.Sp), trabecular number (Tb.Tn), and object surface/volume ratio (BS/BV).

Transmission electron microscopy assay
To investigate the mitochondrial morphology changes, C3H10T1/2 cells were collected and pre-treated with 3% glutaraldehyde. The specimens were subsequently fixed in 1% osmium tetroxide, dehydrated in a series of graded acetone solutions, infiltrated with Epon 812 for extended periods, and then embedded. Semi-transparent sections were stained with methylene blue, ultra-thin sections were cut using a diamond knife, and further stained with uranyl acetate and lead citrate. The sections were examined using a JEM-1400-FLASH transmission electron microscope.

Cell viability assay
To assess the effects of DEX, RSL3, and Ferrostatin-1 on cell viability, the Cell Count Kit (CCK-8) (C0037, Beyotime, Shanghai, China) was employed. C3H10T1/2 cells were seeded in 96-well plates at a density of 5000 cells per well. Subsequently, cells were treated with varying concentrations of DEX (10^{-9}, 10^{-8}, 10^{-7}, 10^{-6}, and 10^{-5} M), RSL3 (0, 0.1, 0.5, 1, 2, 4, and 8 μM), or Ferrostatin-1 (0, 0.5, 1, 2, 4, 8, and 16 μM) for either 24–48 h. Then, cells

were incubated with CCK8 mixed solution in the dark at 37 °C for 30 min. Finally, the absorbance of each well was measured at 450 nm using a microplate reader (Thermo, USA).

A Calcein-AM/PI kit (C2015-M, Beyotime, Shanghai, China) was used following the manufacturer's protocol for live/dead staining. Cells were seeded at a concentration of 20,000 cells per well in a 24-well plate and treated with medium containing DEX or AdPDK4 for 48 h. Subsequently, the working solution was added, and cells were incubated at 37 °C for 30 min before imaging under a fluorescence microscope (Olympus, Japan).

Intracellular iron ions, ROS, and malondialdehyde assay
The detection of total intracellular iron ions was performed using the Total Iron Content Colorimetric Assay Kit (E1042, Applygen, Beijing, China). Levels of ROS were assessed utilizing either DCFH-DA (S0033S, Beyotime, Shanghai, China) or DHE (S0063, Beyotime, Shanghai, China) fluorescent probes. Measurement of malondialdehyde (MDA) content was conducted with a lipid oxidation detection kit (S0131S, Beyotime, Shanghai, China). Each specific experimental procedure was executed according to the manufacturer's instructions, with analysis conducted using either an enzyme-linked immunosorbent assay (Thermo, USA) or a fluorescence microscope (Olympus, Japan).

Plasma PDK4, GSH, MDA, and ROS assay
Freshly collected blood underwent natural coagulation for 30 min followed by centrifugation at 4 °C for 10 min to obtain the supernatant (serum). The concentrations of PDK4, GSH, and MDA in the serum were determined using an enzyme-linked immunosorbent assay (ELISA) kit (Ruixinbio, Quanzhou, China). Absorbance was measured at 450 nm using a microplate reader, and optical density (OD) values were converted to concentrations. For ROS analysis, absorbance was measured using a fluorescent enzyme-linked immunosorbent assay (ELISA) with an excitation wavelength of 535 nm and an emission wavelength of 610 nm, employing the reactive oxygen species O13 fluorescence probe method. The OD values were then converted into concentrations. Specifically, the OD values obtained from calibration with a standard sample were converted into concentrations using a formula derived from the standard sample.

Molecular docking
Molecular docking was performed to assess the binding affinity of dexamethasone with potential targets, indicative of its stability. Protein molecular structures of the potential targets were downloaded from the PDB database (https://www.rcsb.org/), while the structure of dexamethasone was obtained from the PubChem database (

https://pubchem.ncbi.nlm.nih.gov/). The structures of the potential targets and dexamethasone were imported into AutoDock Tools software for processing. Global docking was conducted with 50 random docking runs to ensure thorough exploration of binding configurations. The docking result with the lowest binding energy was selected for further analysis. Visualization of the docking outcome was achieved using PyMol 2.5.5.

Statistical analysis

The data were expressed as mean ± standard error, and all experiments are repeated independently at least three times. The experimental data was analyzed using Graph-Pad Prism 9.5.0 software, and western blot images, ALP staining images, ARS staining images, and partial fluorescence images were quantified using Image J software. The differences between two groups were statistically analyzed using two-tailed Student's t-test, and one-way ANOVA was used for comparison between two or more groups. If the P value is less than 0.05, the difference is considered statistically significant.

The work has been reported in line with the ARRIVE guidelines 2.0.

Results

Effects of DEX on osteogenic differentiation of MSCs

Given that DEX is also one of the components of osteogenic induction medium, we prepared DEX at concentrations of 10^{-9} M ~ 10^{-5} M to induce osteogenic differentiation, and screened the appropriate concentration of DEX to inhibit osteogenic differentiation based on the preliminary results for the subsequent experiments. The results of ALP and Alizarin Red staining showed that low concentrations of DEX (10^{-9} M, 10^{-8} M, 10^{-7} M) increased ALP activity compared to the DMEM group, while high concentrations of DEX (10^{-6} M, 10^{-5} M) significantly inhibited OIM-induced ALP activity (Fig. 1A, B) and the level of matrix mineralization (Fig. 1C, D). Next, we chose 10^{-6} M DEX for subsequent experiments. RT-qPCR and western blot results showed that high concentrations of DEX could significantly reduce the mRNA and protein levels of RUNX2 (Fig. 1E-G) and OPN (Fig. 1H-J) induced by OIM.

Effects of GIOP and/or osteogenic induction on the expression of PDK4

To understand the mechanism through which DEX regulates osteogenic differentiation, we performed transcriptome sequencing after using BMP9 as an osteogenic induction model and treating MSCs with 10^{-6} M DEX. Differential gene analysis was performed with P value of < 0.05 and ∣LogFC∣ ≥1. Volcano plots and differential gene heatmap analyses showed that PDK4 was significantly upregulated by DEX (Fig. 2A, B). RT -qPCR

results showed that PDK4 was expressed in different tissues and stem cells (Fig. S1A, B). Given the widespread use of C3H10T1/2 cells in osteogenic differentiation studies, we used this cell line in our subsequent experiments. We examined the changes of PDK family members under osteogenic induction, and the results showed that the mRNA levels of PDK family were all upregulated under OIM induction, with PDK4 being the most significant (Fig. 2C). Immunohistochemical staining showed that PDK4 was downregulated in the bone tissue of GIOP rats (Fig. 2D). Meanwhile, we found that the mRNA and protein levels of PDK4 were upregulated in a time-dependent manner, peaking on day 7 (Fig. 2E-G). The above results suggested that PDK4 may be involved in the osteogenic differentiation process of MSCs and the pathological process of GIOP. These results suggested that PDK4 may have a promoting effect on the GCs-induced inhibition of osteogenic differentiation in MSCs.

Effects of PDK4 on DEX-inhibited osteogenic differentiation

To accurately determine the role of PDK4 in osteogenic differentiation, we employed a concentration of 10^{-6} M DEX for subsequent experiments. RT-qPCR and western blot results showed that PDK4 partially reversed the mRNA and protein levels of RUNX2 (Fig. 3A-C) and OPN (Fig. 3F-H) that were reduced by DEX. Additionally, ALP and ARS staining results showed that the ALP activity (Fig. 3D, E) and cellular matrix mineralization levels (Fig. 3I, J) inhibited by DEX were partially restored by PDK4. These results suggested that PDK4 can mitigate the DEX-inhibited osteogenic differentiation of MSCs.

The relationship between the DEX's osteogenic inhibitory effect and ferroptosis in MSCs

As DEX may promote ferroptosis in different cells, we aimed to explore its effect on ferroptosis in MSCs. Calcein/PI staining showed a decrease in the viability of C3H10T1/2 cells upon DEX treatment (Fig. 4A, B). Transmission electron microscopy analysis demonstrated that DEX induced mitochondrial wrinkling and increased membrane density, showing morphological changes of ferroptosis (Fig. 4C). Furthermore, DEX triggered the elevated levels of cellular ROS content (Fig. 4D), MDA content (Fig. 4E) and total iron ion levels (Fig. 4F). RT-qPCR and western blot results showed that DEX downregulated the mRNA and protein levels of the negative regulators of ferroptosis, including GPX4, FTH1 and SLC7A11, but upregulated the ACSL4 mRNA and protein levels of ACSL4 (Fig. 4G, H). RT-qPCR and western blot results showed an increase in both mRNA and protein levels of negative regulators of ferroptosis during the osteogenic differentiation of MSCs in a roughly time-dependent manner (Fig. 4I, J).
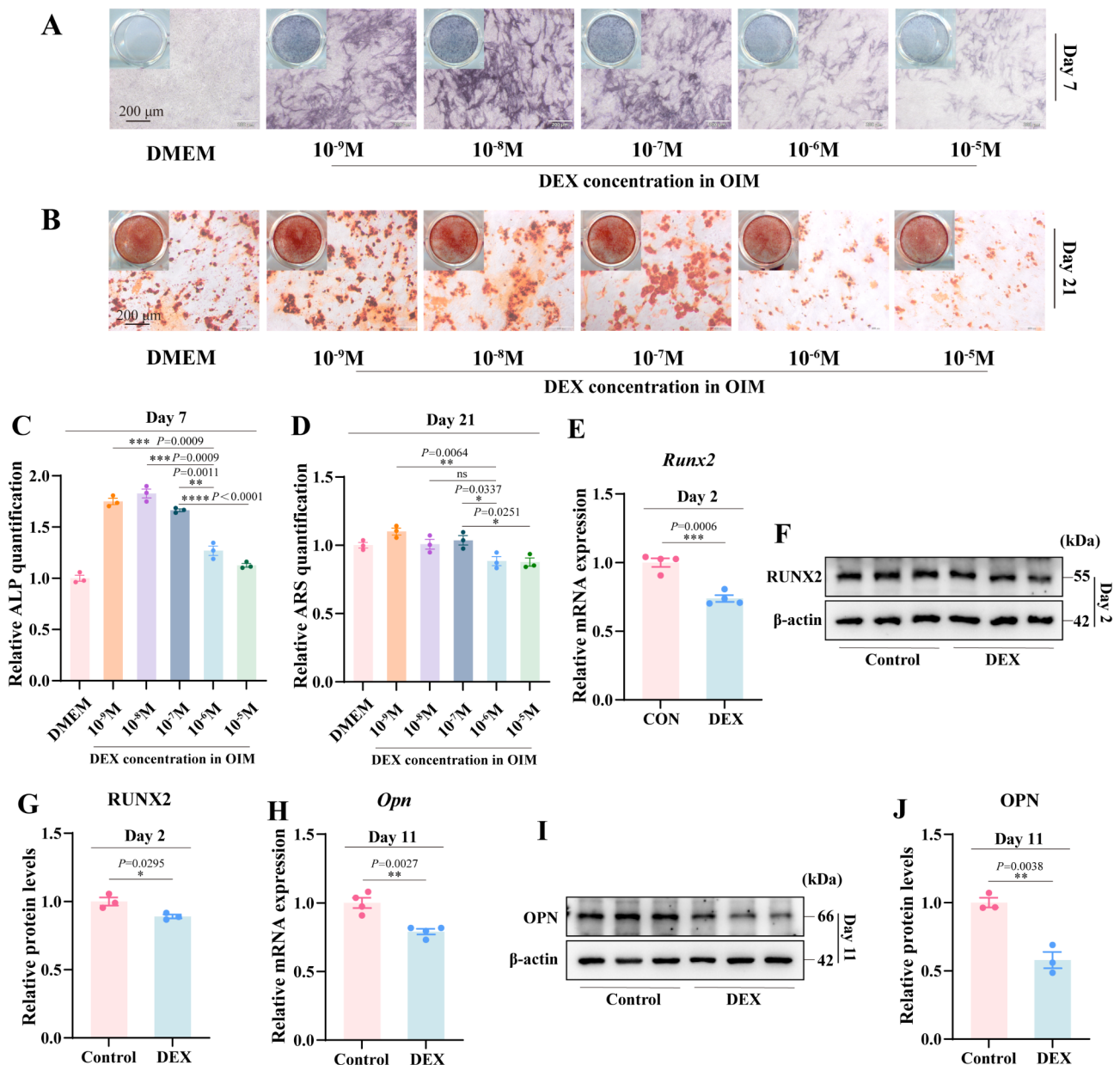
Fig. 1 Effects of DEX on osteogenic differentiation in C3H10T1/2

(**A**-**B**) ALP staining and its quantification showed the effect of different concentrations of DEX on OIM-induced ALP activities in C3H10T1/2 after 5 and 7 days. Scar bar: 200 μm. (**C**-**D**) Alizarin Red S staining and its quantification showed the effect of different concentrations of DEX on OIM-induced matrix mineralization in C3H10T1/2 after 14 and 21 days. Scar bar: 200 μm. (**E**) RT-qPCR detection demonstrated the effect of high concentration of DEX (10^{-6} M) on OIM-induced RUNX2 mRNA levels after 1 and 2 days. (**F**-**G**) Western blot results and these quantifications demonstrated the effect of high concentration of DEX (10^{-6} M) on OIM-induced RUNX2 protein levels after 1 and 2 days. (**H**) RT-qPCR detection demonstrated the effect of high concentration of DEX (10^{-6} M) on OIM-induced OPN mRNA levels after 9 and 11 days. (**I**-**J**) Western blot results and these quantifications demonstrated the effect of high concentration of DEX (10^{-6} M) on OIM-induced OPN protein levels after 9 and 11 days. The uncropped gels and blot were shown in supplementary Fig. 1 (Fig. S1). The data for ALP activities on day 5, Runx2 mRNA level on day 1, mRNA and protein level for OPN on day 9, and Alizarin Red S staining on day 14 were shown in supplementary Fig. 9 (Fig. S9)

We employed the RSL3 (ferroptosis inducer, data are not shown) and Fer-1 (ferroptosis inhibitor) to further investigate the relationship between ferroptosis and DEX-inhibited osteogenic differentiation in MSCs. RT-qPCR and western blot results showed that the decrease of RUNX2 mRNA and OPN protein levels induced by DEX were partially reversed by the Fer-1 (Fig. 4K, M). ALP staining and ARS staining further demonstrated that the decrease in ALP activity and matrix mineralization levels caused by DEX were also partially restored
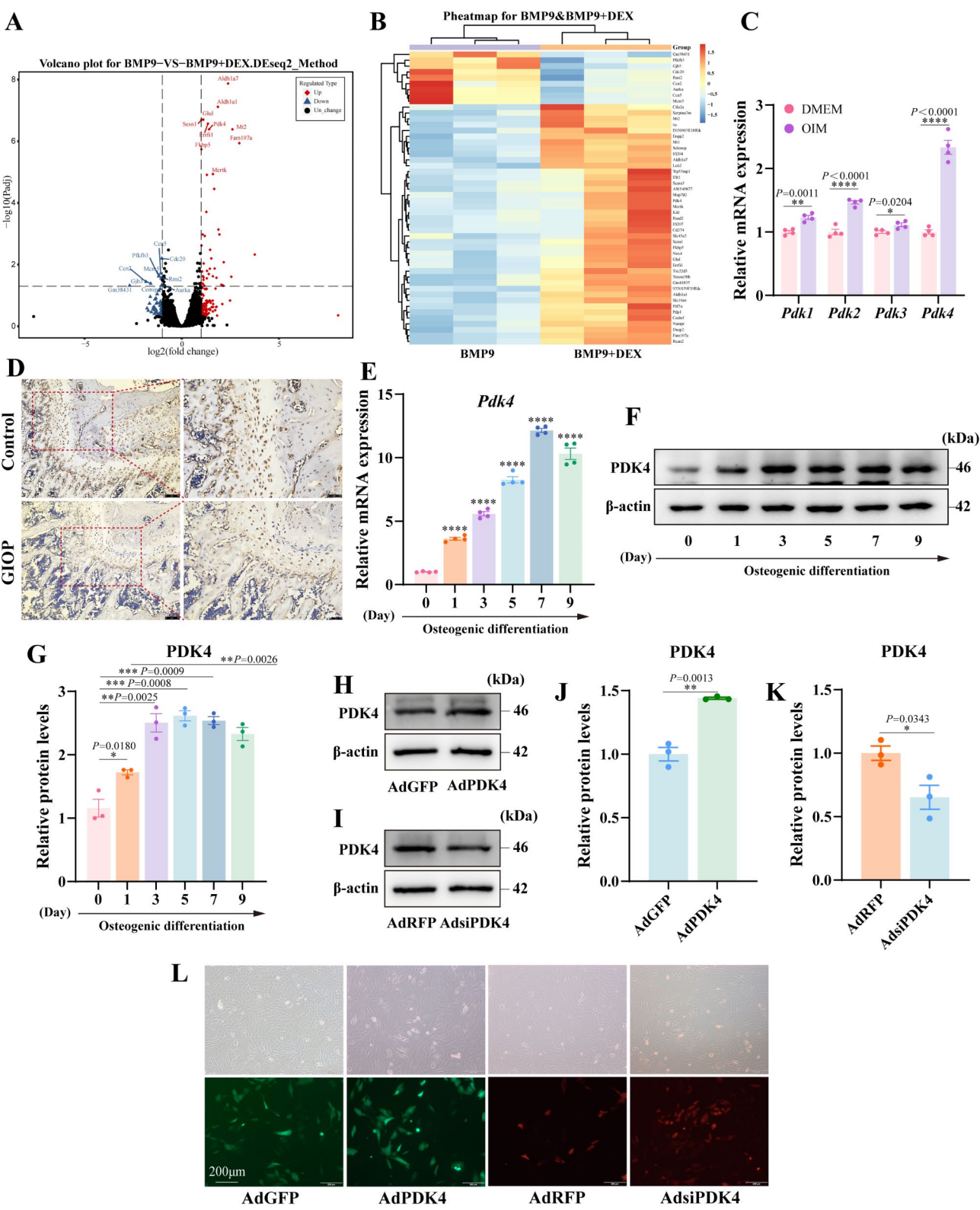
Fig. 2 (See legend on next page.)

(See figure on previous page.)

Fig. 2 Effects of GIOP and/or osteogenic induction on the expression of PDK4

(**A-B**) BMP9 was used as an osteogenic induction model and MSCs were treated with 10^{-6} M DEX before transcriptome sequencing. Differential gene analysis was performed with P value < 0.05 and| LogFC| ≥ 1. Volcano plot and differential gene heatmap analysis showed significantly upregulated or downregulated differentially expressed genes. (**C**) RT-qPCR detection showed the mRNA levels of PDK family members in C3H10T1/2 cells after OIM treated for 2 days. (**D**) Immunohistochemical staining results showed the level of PDK4 in the tibia of GIOP model. Scar bar: 50 μm. (**E**) PCR assay showed the expression of *Pdk4* during osteogenic differentiation in MSCs. (**F**) Western blot assay showed the protein level of PDK4 during osteogenic differentiation in C3H10T1/2 cells. (**G**) Quantitative results of western blot assay showed the protein level of PDK4 during osteogenic differentiation in MSCs. (**H-I**) Western blot showed the protein expression of PDK4 in C3H10T1/2 after Ad-GFP, Ad-PDK4, Ad-RFP and Ad-siPDK4 infection. (**J-K**) Quantitative analysis results of western blot showed the protein expression of PDK4 in C3H10T1/2 after Ad-GFP, Ad-PDK4, Ad-RFP and Ad-siPDK4 infection. (**L**) Microscopic white light and fluorescence images of C3H10T1/2 infected with adenovirus-mediated Ad-GFP, Ad-PDK4, Ad-RFP, and Ad-siPDK4 after 24 h. Scar bar: 200 μm. The uncropped gels and blot were shown in supplementary Fig. 2 (Fig. S2)

by Fer-1. However, there were no significant changes in ALP activity and matrix mineralization levels in the Fer-1 alone treatment group compared to the control group (Fig. 4L, N). These results suggested a potential association between the DEX-inhibited osteogenic differentiation and the promotion of ferroptosis in MSCs.

Effects of PDK4 on DEX-induced ferroptosis in MSCs

Subsequently, we explored whether PDK4 could affect ferroptosis induced by DEX in MSCs. The transmission electron microscopy results indicated that PDK4 partially mitigated the DEX-induced morphological alterations such as mitochondrial wrinkling and increased membrane density (Fig. 5A). Assessment of total iron ion and MDA levels revealed that PDK4 attenuated the DEX-induced increase in MDA and total iron ion levels (Fig. 5B, C). DHE staining showed that PDK4 partially reversed the increase of ROS content caused by DEX (Fig. 5D). The further western blot results showed PDK4 inhibited the increase of ACSL4 protein levels caused by DEX, reversed the decrease of GPX4 and SLC7A11 protein levels caused by DEX, but no significant effect on protein levels of FTH1 (Fig. 5E-I). These results suggested that PDK4 can inhibit the DEX-induced ferroptosis in MSCs.

Effects of PDK4 on bone formation and ferroptosis in GIOP rats

To assess the effect of PDK4 on the bone damage effect of DEX, we established a GIOP rat model. Masson's trichrome staining showed a notable reduction in bone trabecular density and collagen fiber production in the GIOP and viral empty vector groups relative to the control group. Conversely, PDK4 overexpression led to augmentation of collagen fiber production and increased-density of bone trabeculae (Fig. 6A). Micro-CT scans confirmed a decreased density of bone trabeculae in the GIOP and viral empty vector groups compared to controls, which was significantly attenuated by PDK4 overexpression (Fig. 6B). Quantitative analyses results of bone trabecular parameters were consistent with the micro-CT results (Fig. 6C-G). Furthermore, we determined the impact of PDK4 on ferroptosis-related

markers. ELISA results showed a decrease in glutathione content and an increase in malondialdehyde content in the GIOP model group compared to controls, which was partially reversed by PDK4 overexpression (Fig. 6H, I). O13 probe detection revealed that PDK4 overexpression attenuated the heightened ROS content in the GIOP model group compared to controls (Fig. 6J). Western blot analysis exhibited an elevated ACSL4 protein levels but decreased levels of GPX4, SLC7A11, and FTH1 in the femur of the GIOP model group compared to controls. PDK4 overexpression partially reversed these alterations, albeit without statistical significance in SLC7A11 protein levels (Fig. 6K, L). These results suggested that PDK4 has an ameliorative effect on GIOP via reducing ferroptosis.

Effects of ferroptosis on the attenuation of DEX-inhibited osteogenic differentiation by PDK4 in MSCs

To further investigate whether the reversal effect of PDK4 on DEX inhibition of MSCs osteogenic differentiation is related to ferroptosis, we employed a ferroptosis inducer (RSL3) for pertinent experiments. RT-qPCR and western blot analyses revealed that the reversal effect of PDK4 on the mRNA and protein levels of RUNX2 (Fig. 7A-C) and OPN (Fig. 7F-H) caused by DEX was partially offset by RSL3. ALP staining showed that RSL3 partially counteracted PDK4's ability to reverse the decrease in ALP activities induced by DEX, with more pronounced effects observed on day 7 (Fig. 7D, E). Additionally, ARS staining results showed that the effect of PDK4 on inhibiting the DEX-caused matrix mineralization decrease were partially attenuated by RSL3 (Fig. 7I, J). These results suggested that the reversal effect of PDK4 on the DEX's inhibitory effect on osteogenic differentiation in MSCs was mediated by disturbing ferroptosis partially.

Effects of DEX on *Pdk4* mRNA expression and protein degradation in MSCs

Although we have demonstrated the role of PDK4 in reducing the DEX-caused reduction of osteogenic differentiation, the interaction between DEX and PDK4 remains unclear. Thus, we analyzed the effects of DEX on PDK4 expression. RT-qPCR and western blot analyses showed an upregulation of PDK4 mRNA levels
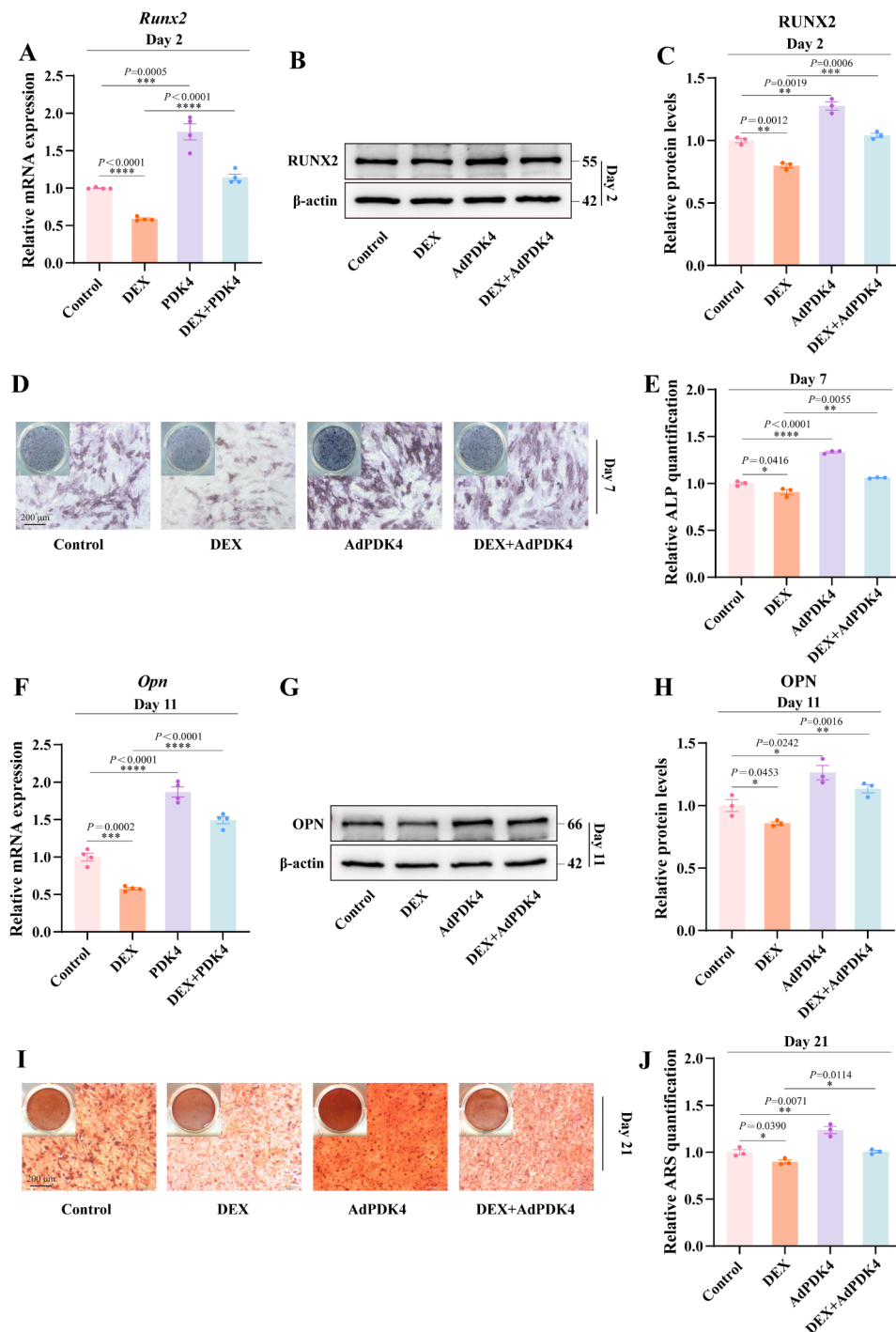
Fig. 3 Effects of PDK4 on DEX-inhibited osteogenic differentiation

(**A**) RT-qPCR results showed the effect of AdPDK4 and/or DEX on RUNX2 mRNA levels after 1 and 2 days. (**B-C**) Western blot results and these quantifications demonstrated the effect of AdPDK4 and/or DEX on RUNX2 protein levels after 1 and 2 days. (**D-E**) ALP staining and its quantification showed the effect of AdPDK4 and/or DEX on ALP activities after 5 and 7 days. Scar bar: 200 μm. (**F**) RT-qPCR results showed the effect of AdPDK4 and/or DEX on OPN mRNA levels after 9 and 11 days. (**G-H**) Western blot results and these quantifications demonstrated the effect of AdPDK4 and/or DEX on OPN protein levels after 9 and 11 days. (**I-J**) Alizarin Red S staining and its quantification showed the effect of AdPDK4 and/or DEX on matrix mineralization levels after 14 and 21 days. Scar bar: 200 μm. The uncropped gels and blot were shown in supplementary Fig. 3 (Fig. S3). The data for ALP activities on day 5, Runx2 mRNA level on day 1, mRNA and protein level for OPN on day 9, and Alizarin Red S staining on day 14 were shown in supplementary Fig. 10 (Fig. S10)
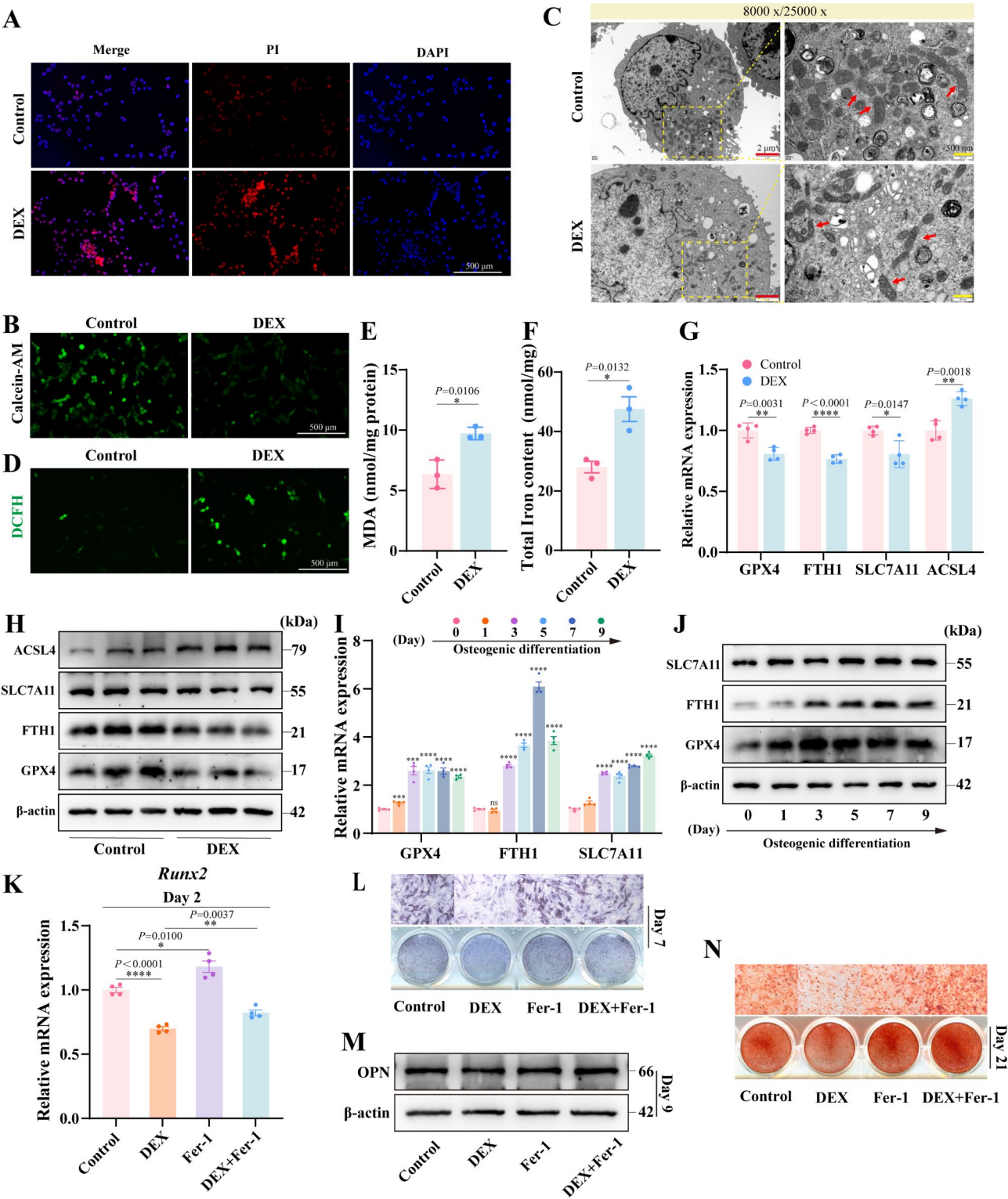
Fig. 4 (See legend on next page.)

across different DEX concentrations compared to the DMEM control group (Fig. 8A). However, the protein level of PDK4 was increased by low concentrations (10^{-9} M, 10^{-8} M, 10^{-7} M) of DEX, but decreased by high concentrations (10^{-6} M, 10^{-5} M) of DEX compare to the control group (Fig. 8B, C). To further elucidate the underlying mechanism, we investigated whether DEX could influence the degradation of PDK4 protein. Western blot

(See figure on previous page.)

Fig. 4 Effects of DEX on ferroptosis and the relationship between ferroptosis and osteogenic differentiation of MSCs
(**A**, **B**) The Calcein-AM/PI staining results showed fluorescence images of cell viability in C3H10T1/2 cells treated with DMSO or 1 μM DEX for 48 h. Scar bar: 500 μm. (**C**) Transmission electron microscopy observations showed the effect of 1 μM DEX treatment for 48 h on mitochondrial morphology in C3H10T1/2 cells. Red scar bar: 2 μm. Yellow scar bar: 500 nm. (**D**) Effect of DEX on reactive oxygen species generation detected by 2′,7′-dichlorodihydrofluorescein diacetate probe. Scar bar: 500 μm. (**E**) MDA detection assay showed the effect of DEX on lipid peroxidation level. (**F**) Total iron colorimetric assay showed the effect of DEX on intracellular iron content. (**G-H**) RT-qPCR and Western blot analysis showed the effect of DEX on mRNA and protein level of ferroptosis key factors. (**I-J**) RT-qPCR and Western blot analysis showed changes in ferroptosis key factors during osteogenic differentiation of C3H10T1/2 cells. (**K**) RT-qPCR detection indicated the effect of 5 μM Fer-1 on DEX inhibited RUNX2 mRNA level after 1 and 2 days. (**L**) ALP staining showed the effect of 5 μM Fer-1 on DEX inhibited ALP activity after 7 days. Scar bar: 200 μm. (**M**) Western blot analysis showed the effect of 5 μM Fer-1 on DEX inhibited OPN protein level after 9 days. (**N**) Alizarin Red S staining showed the effect of 5 μM Fer-1 on DEX inhibited matrix mineralization levels after 14 and 21 days. Scar bar: 200 μm. The uncropped gels and blot were shown in supplementary Fig. 4 (Fig. S4). The data for Runx2 mRNA level on day 1 and Alizarin Red S staining on day 14 were shown in supplementary Fig. 11 (Fig. S11)

analyses showed that DEX accelerated PDK4 degradation compared to cycloheximide (CHX) treatment alone (Fig. 8D-F). Given that protein degradation primarily occurs via the ubiquitin-proteasome or autophagy-lysosomal pathways, we utilized the proteasome inhibitor MG132 and the autophagy inhibitor bafilomycin A1 (BafA1) to analyze potential degradation measure facilitated by DEX. Western blot assay showed that BafA1 effectively rescued the reduction in PDK4 protein levels induced by DEX, whereas MG132 did not yield the similar effect (Fig. 8G, H). Laser confocal images more visually showed the increased translocation of PDK4 protein to the lysosome after DEX (10^{-6} M) treatment compared to control (Fig. 8I). The molecular docking analysis indicated the stable binding between DEX and PDK4, with DEX predominantly interacting with ASN-187 and HIS-190 residues of PDK4 in the lowest-energy binding mode (Fig. 8J). These results suggested that the inhibitory effect of high concentration or dose of DEX on osteogenesis may be achieved by promoting the PDK4 degradation through lysosomal pathway, and thereby lead to ferroptosis in MSCs.

Discussion

It is universally acknowledged that prolonged or excessive exposure to glucocorticoids (GCs) elicits bone harm, yet the precise molecular underpinnings of this detrimental effect remain elusive. A pivotal function of GCs involves elevating serum glucose levels, and the osteogenic capacity of mesenchymal stem cells (MSCs) is susceptible to alterations mediated by distinct glucose metabolic pathways. Notably, PDK4 modulates the glucose metabolic profile by directing the flux of pyruvate. Herein, we delved into the potential involvement of ferroptosis in GC-mediated bone damage, specifically examining the role of PDK4 in this process. Our findings revealed that augmented ferroptosis is intimately linked to bone damage induced by DEX (10^{-6} M), a type of GCs, and this damage can be partially mitigated by PDK4. Furthermore, DEX may diminish PDK4 level via a nongenomic mechanism by binding with it directly.

GCs, such as DEX, has been widely used since the 1940s for the treatment of autoimmune diseases, asthma, and chronic inflammatory diseases [35, 36]. However, the prolonged usage of GCs has been related to serious skeletal complications, with fractures occurring in approximately 40% of these patients [37]. Studies have reported that GCs play an important role in regulating MSC differentiation at physiological concentrations [38], such as promote osteogenic differentiation of MSCs [39]. Whereas high concentrations of DEX (1 μM) increase the lipogenic differentiation of MSCs while attenuating their ability to differentiate towards osteogenic lineage [40–42], and most of these effects are associated with altered Wnt/β-catenin signaling [8, 9]. DEX is one of the major components of OIM, and the concentrations of DEX commonly used to induce osteogenic differentiation of MSCs are 10^{-9} M, 10^{-8} M and 10^{-7} M, but there is no consensus on the optimal concentration [43]. In this study, we used OIM containing 10^{-7} M DEX. We found that the osteogenic induction effect of different concentrations of DEX on MSCs varied due to differences in treatment time. For example, the ALP activity of MSCs induced by OIM containing 10^{-9} M and 10^{-8} M DEX for 5 days was higher than that of 10^{-7} M, but there was no significant difference after 7 days. This highlights the dynamic interaction of DEX concentration, exposure time and cell types. Consistent with previous reports, our results showed that low concentrations of DEX promoted ALP activity and matrix mineralization, whereas high concentrations (10^{-6} M, 10^{-5} M) of DEX significantly reduced the mRNA and protein levels of RUNX2 and OPN, inhibited ALP activity and matrix mineralization levels; Meanwhile, animal experiments have also confirmed that DEX induces osteoporosis in rats, leading to a decrease in bone density and trabecular bone.

PDK4 is a key enzyme that regulates the activity of the pyruvate dehydrogenase complex (PDC) and inhibits its activity by phosphorylating its subunits, reducing the production of acetyl coenzyme A and promoting glycolysis [17–19]. Aerobic glycolysis plays an important role in the osteogenic differentiation of MSCs [15, 16], and the impact of glycolysis on the osteogenic differentiation of
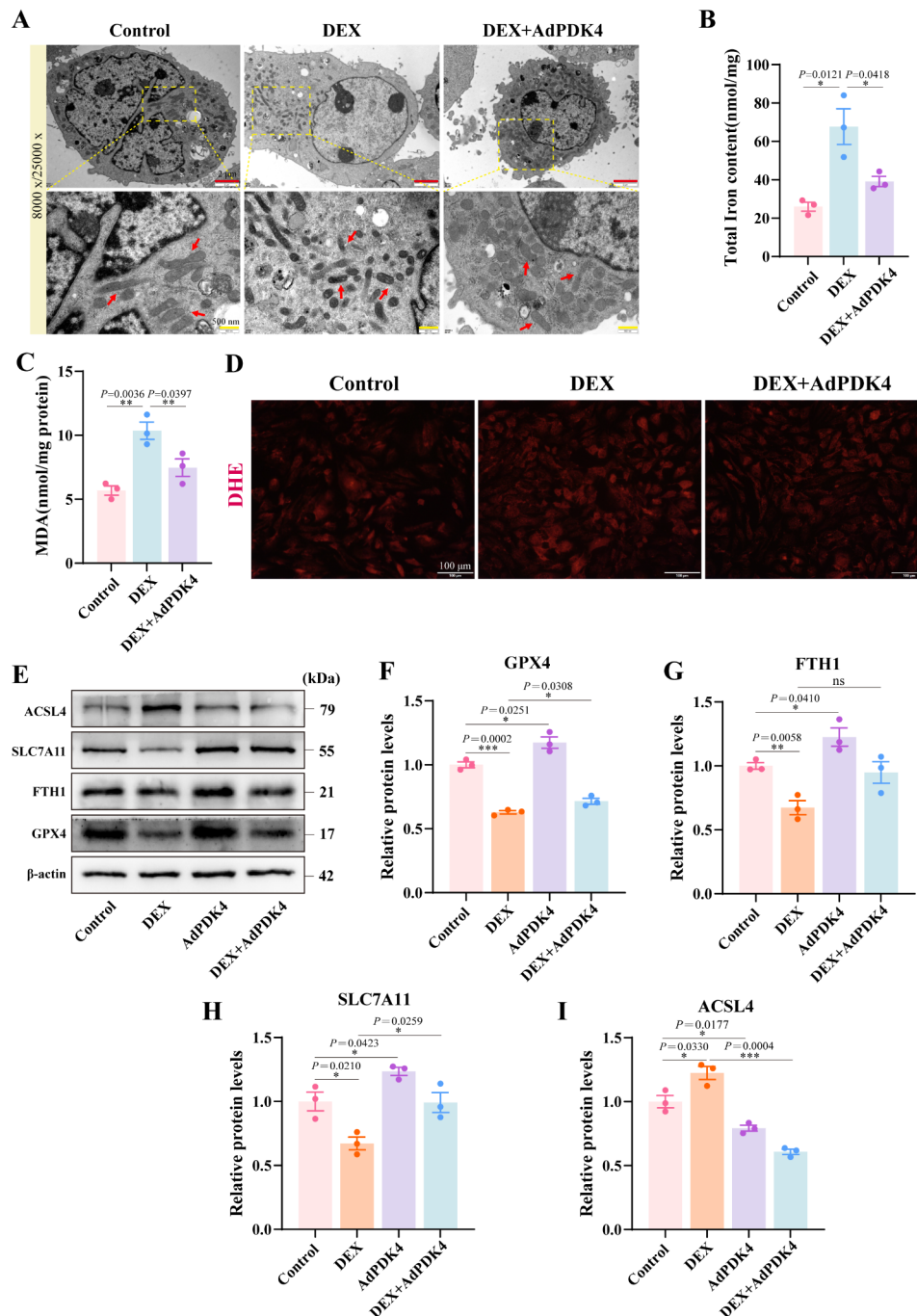
Fig. 5 Effects of PDK4 on DEX-induced ferroptosis in MSCs

(**A**) Transmission electron microscopy observation revealed the effect of AdPDK4 and DEX on mitochondrial morphology in C3H10T1/2 cells (Red scar bar: 2 μm. Yellow scar bar: 500 nm). (**B**) Total iron colorimetric assay showed the effect of AdPDK4 and DEX on on intracellular iron content. (**C**) MDA detection assay showed the effect of AdPDK4 and DEX on lipid peroxidation level. (**D**) Effect of AdPDK4 and DEX on reactive oxygen species generation detected by dihydroethidium probe. Scar bar: 100 μm. (**E-I**) Western blot analysis and these quantifications showed the effect of AdPDK4 and DEX on protein levels of ferroptosis key factors. The uncropped gels and blot were shown in supplementary Fig. 5 (Fig. S5)

MSCs is related to the plasticity of stem cell fate and glucose metabolism [16, 44]. PDK4 can promote calcification of VSMCs, and vascular calcification is a process similar to bone formation [20, 21]. Our previous studies found that PDK4 can negatively regulate SOST expression and enhance Wnt/β-catenin signaling pathway to promote BMP9-induced osteogenic differentiation by interacting with p-Smad1/5/9 [23]. In this study, our data showed that among the PDK family, the mRNA level of PDK4 changes most significantly under OIM conditions, with
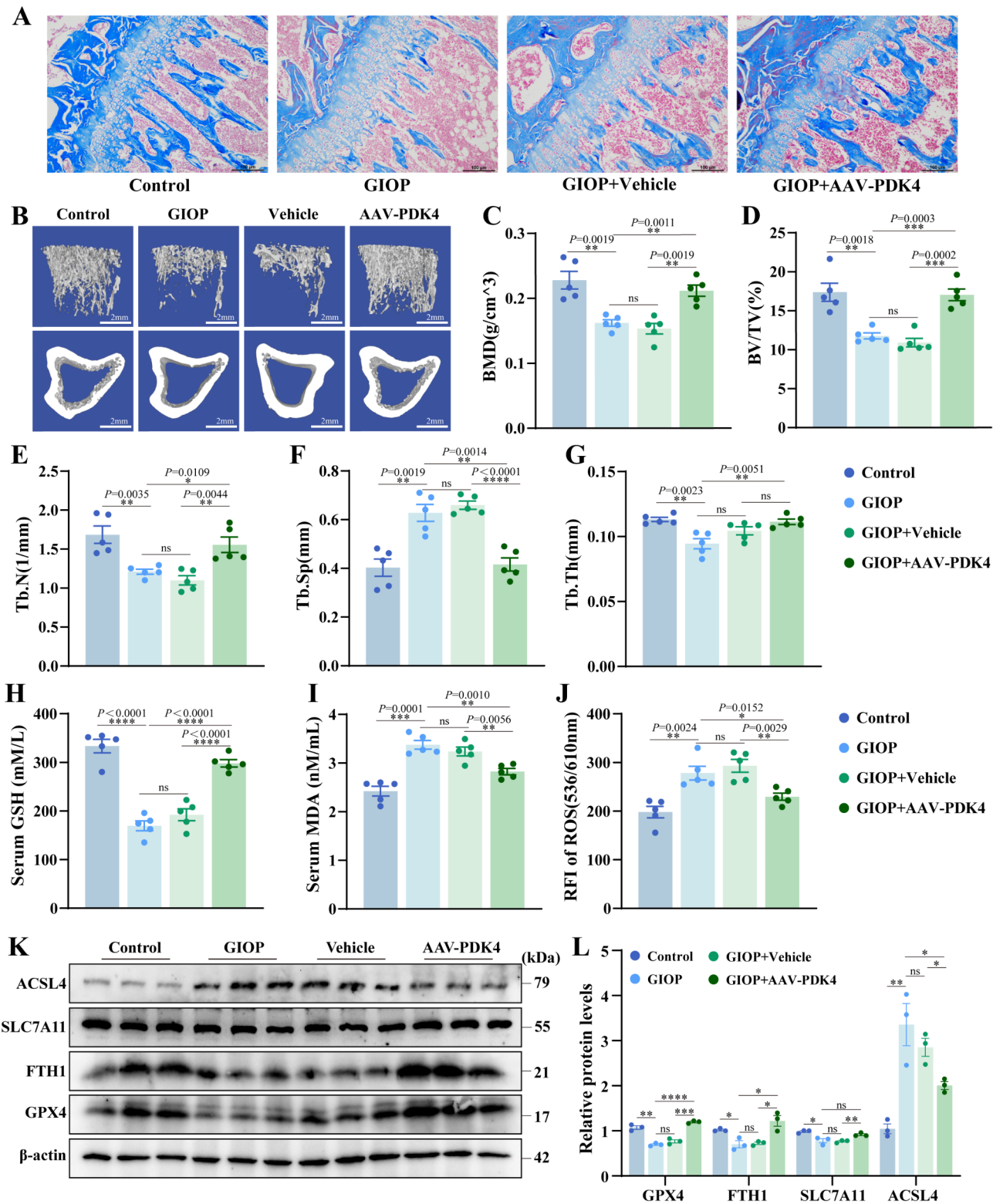
Fig. 6 (See legend on next page.)

(See figure on previous page.)

Fig. 6 Effects of PDK4 on bone formation and ferroptosis in DEX-induced GIOP rats

(**A**) Masson's trichrome staining demonstrated the influence of AAV-PDK4 on collagen fiber synthesis in the tibia of rats with GIOP (Scar bar: 100 μm). (**B**) Micro-CT reconstruction results showed the effect of AAV-PDK4 on the number and density of bone trabeculae in the GIOP rats (Scar bar: 2 mm). (**C-G**) Quantitative analysis of trabecular bone-related indices revealed the effect of AAV-PDK4 on DEX-induced GIOP rats. (**H**) ELISA detection showed the effect of PDK4 on serum glutathione levels in GIOP rats. (**I**) ELISA detection showed the effect of AAV-PDK4 on serum MDA levels in GIOP rats. (**J**) O13 probe detection showed the effect of AAV-PDK4 on serum reactive oxygen species level in GIOP rats. (**K, L**) Western blot analyses and these quantifications showed the effect of AAV-PDK4 on protein levels of ferroptosis key factors in DEX-induced GIOP rats. (*$P < 0.05$, **$P < 0.01$, ***$P < 0.001$, ****$P < 0.0001$ vs. control. BMD, bone mineral density; BV/TV, ratio of bone volume to total volume; Tb.N, trabecular number; Tb.Th, trabecular thickness; Tb.Sp, trabecular separation; AAV-PDK4, adeno-associated virus of PDK4. The uncropped gels and blot were shown in supplementary Fig. 6 (Fig. S6)

a roughly time-dependent manner. Overexpression of PDK4 increased the levels of osteogenic markers, while silencing PDK4 exhibited the opposite effect. We also found that overexpression of PDK4 alleviated the degree of DEX-induced osteoporosis in rats. Therefore, PDK4 may play an important role in preventing osteoporosis from GCs, and PDK4 activators or recombinant proteins may be developed for the treatment of GIOP.

Ferroptosis is closely related to the occurrence and development of orthopedic diseases such as osteoporosis, spinal cord injury, and osteoarthritis [26]. Ferroptosis inhibitors can partially reverse bone loss caused by a high-fat diet [27]. Iron overload can inhibit osteogenic differentiation by inducing ferroptosis in MC3T3-E1 and BMSCs [29, 31]. High concentrations of DEX can induce ferroptosis in BMSCs and MC3T3-E1, and melatonin can inhibit ferroptosis in BMSCs through PI3K/AKT/mTOR signaling, alleviating GIOP [31, 32]. In addition, PDK4 was found to inhibit ferroptosis in human pancreatic cancer and hepatic stellate cells [33, 45]. In this study, we found that high concentrations of DEX (1 μM) can cause mitochondrial damage, induce ROS accumulation, iron accumulation, and lead to ferroptosis in MSCs, but these effects were partially reversed by PDK4. The inhibitory effect of DEX on osteogenic differentiation was partially reversed by the ferroptosis inhibitor Fer-1, whereas the ferroptosis inducer RSL3 attenuated the improvement effect of PDK4 on DEX osteogenic damage. Therefore, our results suggested that PDK4 may improve the osteogenic inhibitory effect of DEX by reducing ferroptosis, providing new insights for the treatment of GIOP.

In exploring how DEX regulates PDK4, our study found that high concentrations of DEX upregulate PDK4 mRNA levels and downregulate its protein levels compared with the OIM control group. The regulatory effect of 10^{-7} M DEX on PDK4 mRNA is consistent with literature reports [46]. DEX shows opposite effects on PDK4 mRNA and protein levels, which may due to the non-genomic effect of high concentrations of DEX, such as promoting post-translational modification of PDK4 protein or directly acting on the protein to accelerate its degradation; thereby, the PDK4 mRNA level can be increased by the feedback regulation. Protein degradation mainly occurs through the ubiquitin proteasome or lysosomal pathways [47]. Our data suggested that DEX

may reduce the protein level of PDK4 by promoting its degradation via lysosomal pathway. However, we have not yet conducted further experimental to verify whether DEX can regulate PDK4 protein level by affecting other factors.

In this study, we utilized RSL3 and Fer-1 to explore the relationship between ferroptosis and DEX-induced osteogenic inhibition. Although the results were convincing, other types of ferroptosis inducers or other cell death pathway inducers were not introduced in our analysis to demonstrate the importance of ferroptosis in osteogenic differentiation. This study needs to be further refined in future studies. In addition, the specific molecular mechanisms of DEX-induced ferroptosis and PDK4 protein degradation need to be further explored.

Conclusion

In summary, our data suggested that DEX can induce ferroptosis in MSCs by down-regulating PDK4 and lead to osteogenic damage. The regulatory effect of DEX on PDK4 may be related to the non-genomic effect by binding with PDK4 and promote its degradation through the lysosomal pathway. Our findings have preliminarily revealed the role of PDK4 in hindering the bone damage effect of GCs, which is beneficial for providing new insights into clinical treatment of GIOP and new targets for drug development.
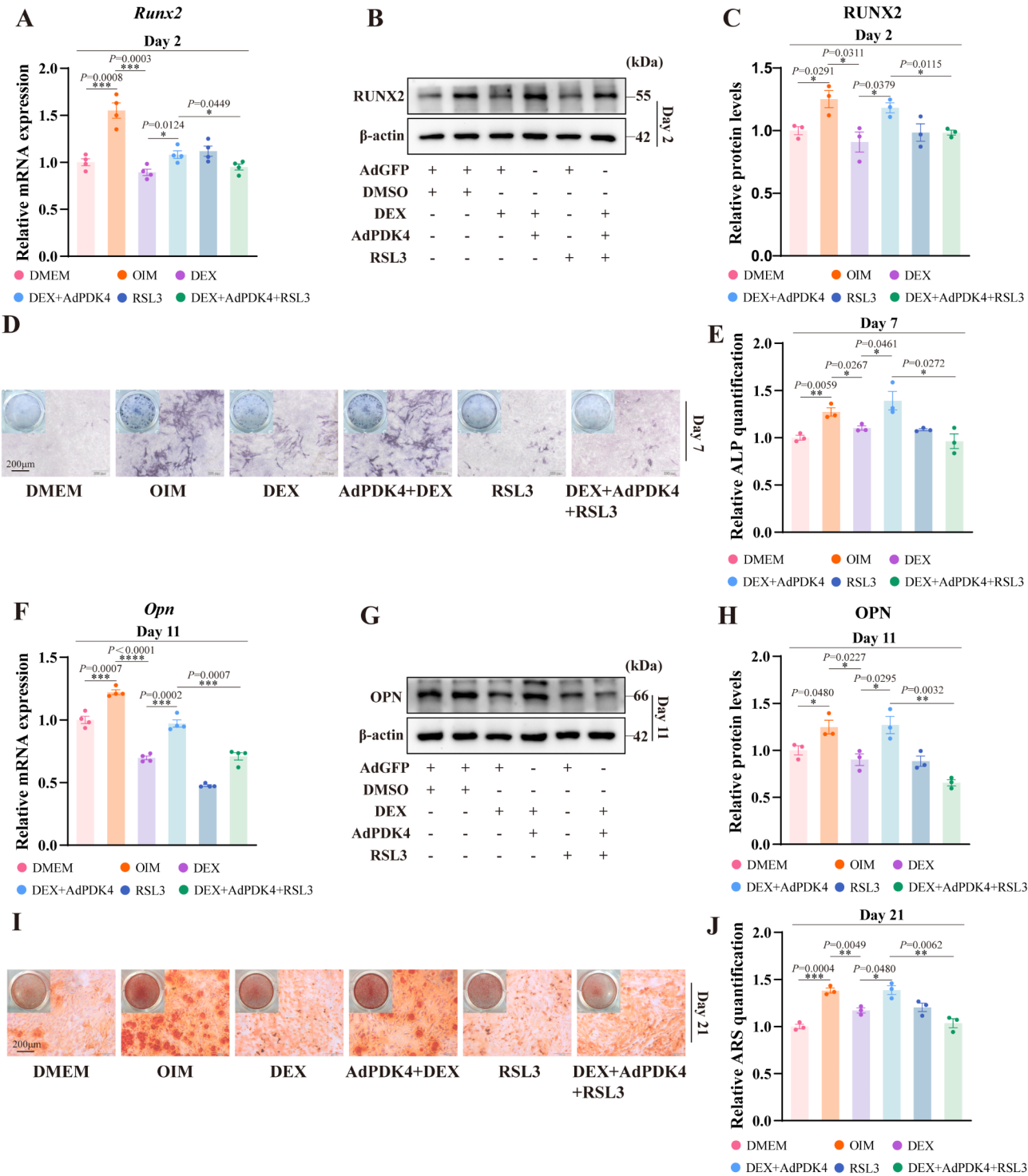
Fig. 7 The relationship between ferroptosis and PDK4 reversal of DEX inhibition of MSCs osteogenic differentiation

(A) RT-qPCR results showed the effect of 2 µM RSL3 on PDK4 reversing DEX-inhibited RUNX2 mRNA levels after 1 and 2 days. (B-C) Western blot results and these quantifications demonstrated the effect of 2 µM RSL3 on PDK4 reversing DEX-inhibited RUNX2 protein levels after 1 and 2 days. (D-E) ALP staining and its quantification showed the effect of 2 µM RSL3 on PDK4 reversing DEX-reduced ALP activities after 5 and 7 days (Scar bar: 200 µm). (F) RT-qPCR results showed the effect of 2 µM RSL3 on PDK4 reversing DEX-inhibited OPN mRNA levels after 9 and 11 days. (G, H) Western blot results and these quantifications demonstrated the effect of 2 µM RSL3 on PDK4 reversing DEX-inhibited OPN protein levels after 9 and 11 days. (I-J) Alizarin Red S staining and its quantification showed the effect of 2 µM RSL3 on PDK4 reversing DEX-reduced matrix mineralization levels after 14 and 21 days. Scar bar: 200 µm. RSL3, a ferroptosis inducer. The uncropped gels and blot were shown in supplementary Fig. 7 (Fig. S7). The data for ALP activities on day 5, Runx2 mRNA level on day 1, mRNA and protein level for OPN on day 9, and Alizarin Red S staining on day 14 were shown in supplementary Fig. 12 (Fig. S12)
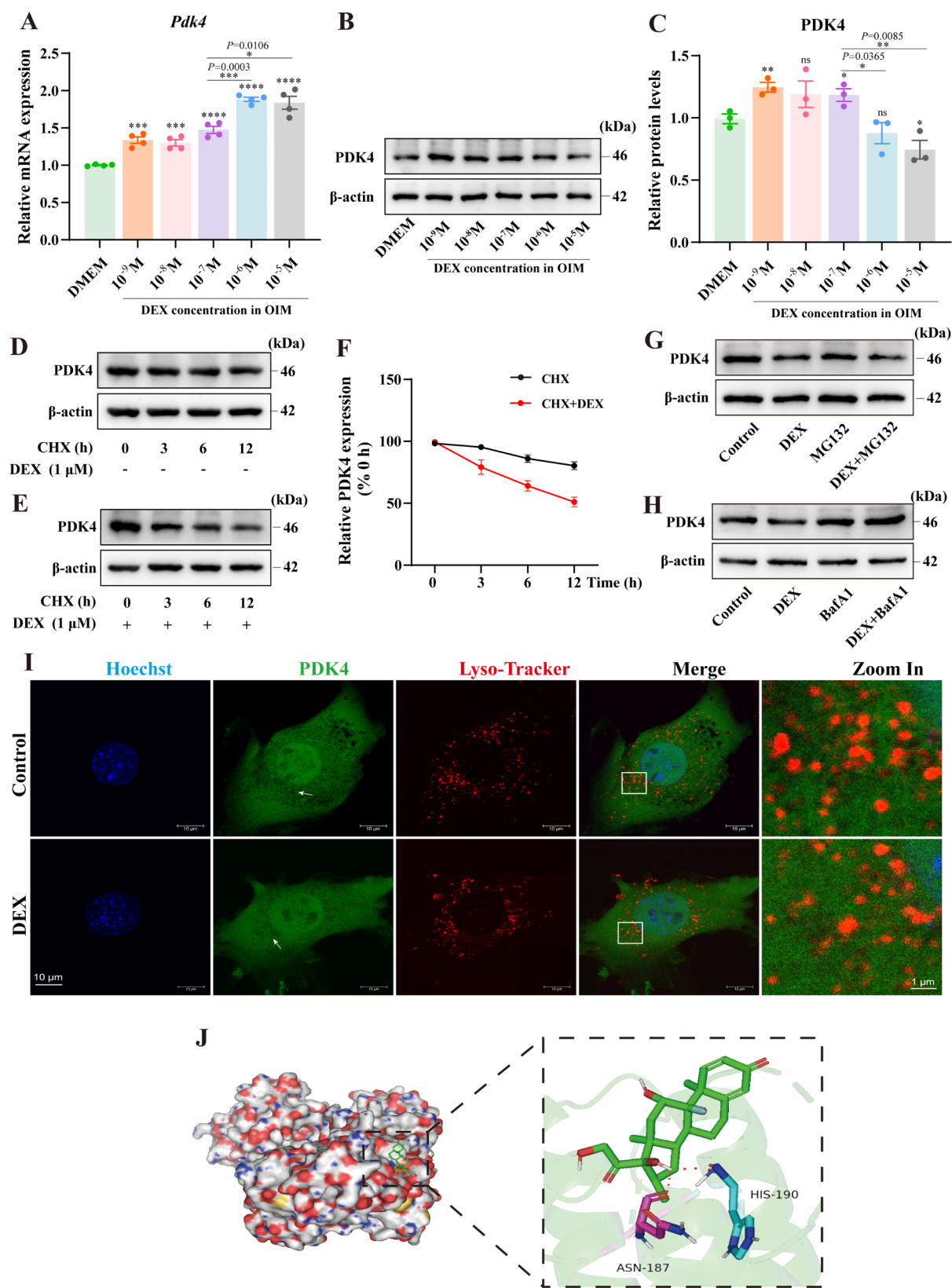
Fig. 8 (See legend on next page.)

(See figure on previous page.)

Fig. 8 Mechanistic studies on the regulation of PDK4 expression by DEX

(**A**) RT-qPCR detection showed the effect of DEX on PDK4 mRNA levels. (**B-C**) Western blot result and its quantification demonstrated the effect of DEX on PDK4 protein levels. (**D, E**) C3H10T1/2 cells were treated with or without 1 µM DEX in the presence of CHX (100 µM) for the indicated time intervals, and the expression of PDK4 was measured by Western blot analysis. (**F**) Relative quantification of the effect of DEX on the degradation rate of PDK4 protein. (**G, H**) Western blot showed the effect of MG132 or BafA1 and DEX on PDK4 protein level. C3H10T1/2 cells were treated with DEX for 48 h, and MG132 was added 6 h before protein extraction. (**I**) Colocalization of PDK4 and lysosomes in C3H10T1/2 cells. AdPDK4 labeled PDK4 as green, lysosomes labeled with lyso-Tracker as red, and finally observed under a laser confocal microscope. (**J**) Molecular docking results for the interaction between DEX and PDK4 protein. CHX: cycloheximide. The uncropped gels and blot were shown in supplementary Fig. 8 (Fig. S8)

Abbreviations

DEX	Dexamethasone
PDK4	Pyruvate dehydrogenase kinase isozyme 4
GIOP	Glucocorticoid-induced osteoporosis
GCs	Glucocorticoids
MSCs	Mesenchymal stem cells
Ad	Adenovirus
AAV	Adeno-associated virus
RUNX2	Runx-related transcription factor 2
OPN	Osteopontin
ARS	Alizarin Red S
ALP	Alkaline phosphatase
BMP9	Bone morphogenetic proteins 9
GPX4	Glutathione peroxidase 4
FTH1	Ferritin heavy chain 1
ACSL4	Acyl-CoA synthetase long chain family member 4
Fer-1	Ferrostatin-1
ROS	Reactive oxygen species
MDA	Malondialdehyde
RFP	Red fluorescent protein
GFP	Green fluorescent protein
OIM	Osteogenic inductive medium
DMEM	Dulbecco's modified Eagle's medium
CHX	Cycloheximide
GSH	Glutathione

Supplementary Information

The online version contains supplementary material available at https://doi.or g/10.1186/s13287-025-04186-9 .

Supplementary Material 1

Supplementary Material 2

Supplementary Material 3

Supplementary Material 4

Supplementary Material 5

Author contributions
BCH, YJ and JW designed this study. YJ, AHY and WGH carried out most of the experiments and data analysis. WGH, LL, XG, and HL helped with animal model and in vivo sample harvest. WTL, FLY, DMH and JYL helped with in vitro experiments and statistical analysis. YJ and AHY prepared the manuscript, BCH and JW helped with paper editing and format revision. The final manuscript was approved by all authors

Data availability
All datasets used and analyzed in study are available from the corresponding author on reasonable request.

Declarations

Ethics approval and consent to participate
The title of the approved project is Study on the effect of Wnt10 and PTEN on BMP9 induced osteogenic differentiation in mesenchymal stem cells. This study was approved by the Ethics Committee of Chongqing Medical University (CQMU). The approval number is IACUC-CQMU-2022-0021, and the data of approval is Dec 31, 2022. This study does not encompass any human samples or data.

The cell lines used in this study, including C3H10T1/2 (CCL-226), 3T3-L1 (CL-173), MC3T3-E1 (CRL-2593), C2C12 (CRL-1772), MEFs (SCRC-1008), and HEK293 (CRL-1573), were obtained from the American Type Culture Collection (ATCC), which has been confirmed that ethical approval was obtained for the collection of these cells. ATCC has also verified that informed consent was obtained from the donors, where applicable, in compliance with relevant ethical guidelines and regulations. For further information, please refer to the vendor's website (https://www.atcc.org/).

Consent for publication
All authors confirm their consent for publication.

Competing interests
The authors declare that they have no competing interest.

Author details
[1]Department of Pharmacology, School of Pharmacy, Chongqing Medical University, No. 1 Yixueyuan Road, Yuzhong District, Chongqing 400016, People's Republic of China
[2]Key Laboratory of Biochemistry and Molecular Pharmacology of Chongqing, Chongqing Medical University, Chongqing 400016, People's Republic of China
[3]Department of Bone and Soft Tissue Oncology, Chongqing University Cancer Hospital, Chongqing 400030, China
[4]Department of Orthropetics, the First Affiliated Hospital of Chongqing Medical University, Chongqing 400016, People's Republic of China
[5]Department of Orthropetics, the Second Affiliated Hospital of Chongqing Medical University, Chongqing 400016, People's Republic of China
[6]Department of Blood Transfusion, the First Affiliated Hospital of Chongqing Medical University, No. 1 Youyi Road, Yuzhong District, Chongqing 400016, People's Republic of China

References
1. Compston J. Glucocorticoid-induced osteoporosis: an update. Endocrine. 2018;61:7–16.
2. Lane NE. Glucocorticoid-Induced osteoporosis: New insights into the pathophysiology and treatments. Curr Osteoporos Rep. 2019;17:1–7.
3. Majumdar S.R., Morin S.N., Lix L.M., Leslie W.D. Influence of recency and duration of glucocorticoid use on bone mineral density and risk of fractures: population-based cohort study. Osteoporos International: J Established as

Result Cooperation between Eur Foundation Osteoporos Natl Osteoporos Foundation USA. 2013;24:2493–8.

4. Huang X, Jie S, Li W, Li H, Ni J, Liu C. Mir-122-5p targets GREM2 to protect against glucocorticoid-induced endothelial damage through the BMP signaling pathway, Molecular and cellular endocrinology, 544 (2022) 111541.

5. Deng S, Dai G, Chen S, Nie Z, Zhou J, Fang H, Peng H. Dexamethasone induces osteoblast apoptosis through ROS-PI3K/AKT/GSK3β signaling pathway. Volume 110. Biomedicine & pharmacotherapy = Biomedecine & pharmacotherapie; 2019. pp. 602–8.

6. Smith E, Redman RA, Logg CR, Coetzee GA, Kasahara N, Frenkel B. Glucocorticoids inhibit developmental stage-specific osteoblast cell cycle. Dissociation of cyclin a-cyclin-dependent kinase 2 from E2F4-p130 complexes. J Biol Chem. 2000;275:19992–20001.

7. Hildebrandt S, Baschant U, Thiele S, Tuckermann J, Hofbauer LC, Rauner M. Glucocorticoids suppress Wnt16 expression in osteoblasts in vitro and in vivo. Sci Rep. 2018;8:8711.

8. Holdsworth G, Greenslade K, Jose J, Stencel Z, Kirby H, Moore A, Ke HZ, Robinson MK. Dampening of the bone formation response following repeat dosing with sclerostin antibody in mice is associated with up-regulation of Wnt antagonists, Bone, 107 (2018) 93–103.

9. Guañabens N, Gifre L, Peris P. The role of wnt signaling and sclerostin in the pathogenesis of glucocorticoid-induced osteoporosis. Curr Osteoporos Rep. 2014;12:90–7.

10. Sun F, Zhou JL, Liu ZL, Jiang ZW, Peng H. Dexamethasone induces ferroptosis via P53/SLC7A11/GPX4 pathway in glucocorticoid-induced osteonecrosis of the femoral head. Biochem Biophys Res Commun. 2022;602:149–55.

11. von Mässenhausen A, Zamora Gonzalez N, Maremonti F, Belavgeni A, Tonnus W, Meyer C, Beer K, Hannani MT, Lau A, Peitzsch M, Hoppenz P, Locke S, Chavakis T, Kramann R, Muruve DA, Hugo C, Bornstein SR, Linkermann A. Dexamethasone sensitizes to ferroptosis by glucocorticoid receptor-induced dipeptidase-1 expression and glutathione depletion. Sci Adv. 2022;8:eabl8920.

12. Liu W, Zhao Z, Na Y, Meng C, Wang J, Bai R. Dexamethasone-induced production of reactive oxygen species promotes apoptosis via endoplasmic reticulum stress and autophagy in MC3T3-E1 cells. Int J Mol Med. 2018;41:2028–36.

13. Wang L, Heckmann BL, Yang X, Long H. Osteoblast autophagy in glucocorticoid-induced osteoporosis. J Cell Physiol. 2019;234:3207–15.

14. Wang T, Liu X, He C. Glucocorticoid-induced autophagy and apoptosis in bone. Apoptosis: Int J Program cell Death. 2020;25:157–68.

15. Dirckx N, Moorer MC, Clemens TL, Riddle RC. The role of osteoblasts in energy homeostasis. Nat Rev Endocrinol. 2019;15:651–65.

16. Lee WC, Guntur AR, Long F, Rosen CJ. Energy Metabolism of the osteoblast: implications for osteoporosis. Endocr Rev. 2017;38:255–66.

17. Smolle M, Prior AE, Brown AE, Cooper A, Byron O, Lindsay JG. A new level of architectural complexity in the human pyruvate dehydrogenase complex. J Biol Chem. 2006;281:19772–80.

18. Guda MR, Asuthkar S, Labak CM, Tsung AJ, Alexandrov I, Mackenzie MJ, Prasad DV, Velpula KK. Targeting PDK4 inhibits breast cancer metabolism. Am J cancer Res. 2018;8:1725–38.

19. Pin F, Novinger LJ, Huot JR, Harris RA, Couch ME, O'Connell TM, Bonetto A. PDK4 drives metabolic alterations and muscle atrophy in cancer cachexia. FASEB Journal: Official Publication Federation Am Soc Experimental Biology. 2019;33:7778–90.

20. Lee SJ, Jeong JY, Oh CJ, Park S, Kim JY, Kim HJ, Doo Kim N, Choi YK, Do JY, Go Y, Ha CM, Choi JY, Huh S, Ho Jeoung N, Lee KU, Choi HS, Wang Y, Park KG, Harris RA, Lee IK. Pyruvate Dehydrogenase Kinase 4 Promotes Vascular Calcification via SMAD1/5/8 Phosphorylation, Scientific reports, 5 (2015) 16577.

21. Kim H, Kim HJ, Lee K, Kim JM, Kim HS, Kim JR, Ha CM, Choi YK, Lee SJ, Kim JY, Harris RA, Jeong D. Lee, α-Lipoic acid attenuates vascular calcification via reversal of mitochondrial function and restoration of Gas6/Axl/Akt survival pathway. J Cell Mol Med. 2012;16:273–86.

22. Yang R, Zhu Y, Wang Y, Ma W, Han X, Wang X, Liu N. HIF-1α/PDK4/autophagy pathway protects against advanced glycation end-products induced vascular smooth muscle cell calcification. Biochem Biophys Res Commun. 2019;517:470–6.

23. Yang YY, Luo HH, Deng YX, Yao XT, Zhang J, Su YX, He BC. Pyruvate dehydrogenase kinase 4 promotes osteoblastic potential of BMP9 by boosting Wnt/β-catenin signaling in mesenchymal stem cells. Int J Biochem Cell Biol. 2023;154:106341.

24. Dixon SJ, Lemberg KM, Lamprecht MR, Skouta R, Zaitsev EM, Gleason CE, Patel DN, Bauer AJ, Cantley AM, Yang WS, Morrison B, Stockwell BR.

25. Jiang X, Stockwell BR, Conrad M. Ferroptosis: mechanisms, biology and role in disease, Nature reviews. Mol cell Biology. 2021;22:266–82.

26. Gao L, Hua W, Tian L, Zhou X, Wang D, Yang Y, Ni G. Molecular mechanism of ferroptosis in Orthopedic diseases. Cells; 2022. p. 11.

27. Lin Y, Shen X, Ke Y, Lan C, Chen X, Liang B, Zhang Y, Yan S. Activation of osteoblast ferroptosis via the METTL3/ASK1-p38 signaling pathway in high glucose and high fat (HGHF)-induced diabetic bone loss. Volume 36. FASEB journal: official publication of the Federation of American Societies for Experimental Biology; 2022. p. e22147.

28. Jiang Z, Wang H, Qi G, Jiang C, Chen K, Yan Z. Iron overload-induced ferroptosis of osteoblasts inhibits osteogenesis and promotes osteoporosis: an in vitro and in vivo study. IUBMB Life. 2022;74:1052–69.

29. Luo C, Xu W, Tang X, Liu X, Cheng Y, Wu Y, Xie Z, Wu X, He X, Wang Q, Xiao Y, Qiu X, Tang Z, Shao G, Tu X. Canonical wnt signaling works downstream of iron overload to prevent ferroptosis from damaging osteoblast differentiation. Volume 188. Free radical biology & medicine; 2022. pp. 337–50.

30. Han L, Wang B, Wang R, Gong S, Chen G, Xu W. The shift in the balance between osteoblastogenesis and adipogenesis of mesenchymal stem cells mediated by glucocorticoid receptor. Stem Cell Res Ther. 2019;10:377.

31. Li M, Yang N, Hao L, Zhou W, Li L, Liu L, Yang F, Xu L, Yao G, Zhu C, Xu W, Fang S. Melatonin Inhibits the Ferroptosis Pathway in Rat Bone Marrow Mesenchymal Stem Cells by Activating the PI3K/AKT/mTOR Signaling Axis to Attenuate Steroid-Induced Osteoporosis, Oxidative medicine and cellular longevity, 2022 (2022) 8223737.

32. Lu J, Yang J, Zheng Y, Chen X, Fang S. Extracellular vesicles from endothelial progenitor cells prevent steroid-induced osteoporosis by suppressing the ferroptotic pathway in mouse osteoblasts based on bioinformatics evidence. Sci Rep. 2019;9:16130.

33. Song X, Liu J, Kuang F, Chen X, Zeh HJ 3rd, Kang R, Kroemer G, Xie Y, Tang D. PDK4 dictates metabolic resistance to ferroptosis by suppressing pyruvate oxidation and fatty acid synthesis. Cell Rep. 2021;34:108767.

34. Li FS, Li PP, Li L, Deng Y, Hu Y, He BC. PTEN reduces BMP9-Induced osteogenic differentiation through inhibiting Wnt10b in mesenchymal stem cells. Front cell Dev Biology. 2020;8:608544.

35. Ahmad M, Hachemi Y, Paxian K, Mengele F, Koenen M, Tuckermann J. A Jack of all trades: Impact of glucocorticoids on Cellular Cross-talk in Osteoimmunology. Front Immunol. 2019;10:2460.

36. Dineen R, Stewart PM, Sherlock M. Factors impacting on the action of glucocorticoids in patients receiving glucocorticoid therapy. Clin Endocrinol. 2019;90:3–14.

37. Chotiyarnwong P, McCloskey EV. Pathogenesis of glucocorticoid-induced osteoporosis and options for treatment. Nat Rev Endocrinol. 2020;16:437–47.

38. Seibel MJ, Cooper MS, Zhou H. Glucocorticoid-induced osteoporosis: mechanisms, management, and future perspectives, the lancet. Diabetes Endocrinol. 2013;1:59–70.

39. Zhou H, Mak W, Zheng Y, Dunstan CR, Seibel MJ. Osteoblasts directly control lineage commitment of mesenchymal progenitor cells through wnt signaling. J Biol Chem. 2008;283:1936–45.

40. Cárcamo-Orive I, Gaztelumendi A, Delgado J, Tejados N, Dorronsoro A, Fernández-Rueda J, Pennington DJ, Trigueros C. Regulation of human bone marrow stromal cell proliferation and differentiation capacity by glucocorticoid receptor and AP-1 crosstalk. J bone Mineral Research: Official J Am Soc Bone Mineral Res. 2010;25:2115–25.

41. He HP, Gu S. The PPAR-γ/SFRP5/Wnt/β-catenin signal axis regulates the dexamethasone-induced osteoporosis. Cytokine. 2021;143:155488.

42. Koromila T, Baniwal SK, Song YS, Martin A, Xiong J, Frenkel B. Glucocorticoids antagonize RUNX2 during osteoblast differentiation in cultures of ST2 pluripotent mesenchymal cells. J Cell Biochem. 2014;115:27–33.

43. Langenbach F, Handschel J. Effects of dexamethasone, ascorbic acid and β-glycerophosphate on the osteogenic differentiation of stem cells in vitro. Stem Cell Res Ther. 2013;4:117.

44. Karner CM, Long F. Glucose metabolism in bone. Bone. 2018;115:2–7.

45. Zhang X, Zhao L, Ying K, Xu J, Huang Y, Zhu R, Ding Y, Cai W, Wu X, Miao D, Xu Q, Zeng Y, Yu F. TUG1 protects against ferroptosis of hepatic stellate cells by upregulating PDK4-mediated glycolysis. Chemico-Biol Interact. 2023;383:110673.

46. Connaughton S, Chowdhury F, Attia RR, Song S, Zhang Y, Elam MB, Cook GA, Park EA. Regulation of pyruvate dehydrogenase kinase isoform 4 (PDK4) gene expression by glucocorticoids and insulin. Mol Cell Endocrinol. 2010;315:159–67.

47. Rusilowicz-Jones EV, Urbé S, Clague MJ. Protein degradation on the global scale. Mol Cell. 2022;82:1414–23.

Publisher's note